

## Research Paper

**Cite this article:** Sieganschin A, Jaschke T, Jacob AF (2021). A compact low-noise frontend for interleaved Rx/Tx arrays at K-/Ka-Band. *International Journal of Microwave and Wireless Technologies* **13**, 595–601. <https://doi.org/10.1017/S1759078721000404>

Received: 30 October 2020  
Revised: 22 February 2021  
Accepted: 3 March 2021  
First published online: 29 March 2021

### Keywords:

Satellite communication (SatCom); phased array; frontend; Rx/Tx-integration; low noise; K-band, Ka-band; full-duplex

### Author for correspondence:

Anton Sieganschin,  
Email: [anton.sieganschin@tuhh.de](mailto:anton.sieganschin@tuhh.de)

© The Author(s), 2021. Published by Cambridge University Press in association with the European Microwave Association. This is an Open Access article, distributed under the terms of the Creative Commons Attribution licence (<http://creativecommons.org/licenses/by/4.0/>), which permits unrestricted re-use, distribution, and reproduction in any medium, provided the original work is properly cited.

# A compact low-noise frontend for interleaved Rx/Tx arrays at K-/Ka-Band

Anton Sieganschin , Thomas Jaschke and Arne F. Jacob

Institut für Hochfrequenztechnik, Techn. Univ. Hamburg, 21073 Hamburg, Germany

## Abstract

This contribution deals with a frontend for interleaved receive (Rx)-/transmit (Tx)-integrated phased arrays at K-/Ka-band. The circuit is realized in printed circuit board technology and feeds dual-band Rx/Tx- and single-band Tx-antenna elements. The dual-band element feed is composed of a substrate-integrated waveguide (SIW) diplexer with low insertion loss, a low-noise amplifier (LNA), a bandpass filter, and several passive transitions. The compression properties of the LNA are identified through two-tone measurements. The results dictate the maximum allowable output power of the power amplifier. The single band feed consists of a SIW with several transitions. Simulation and measurement results of the individual components are presented. The frontend is assembled and measured. It exhibits an Rx noise figure of 2 dB, a Tx insertion loss of ~2.9 dB, and an Rx/Tx-isolation of 70 dB. The setup represents the unit cell of a full array and thus complies with the required half-wave spacing at both Rx and Tx.

## Introduction

Satellite communications (SatCom) are the main technology for providing high-speed Internet access in remote areas and on mobile platforms. So-called Ka-band SatCom links operate at around 20 GHz in downlink and 30 GHz in uplink.

In recent years, phased array antennas for SatCom have been an important research topic and many phased array solutions have been presented. Most often, two separate antennas are utilized for Rx and Tx. Some examples are presented in [1–3]. Highly integrated beamformer network (BN) chips, such as in the literary works [4, 5], are a preferred choice, as they allow to individually tune phase and amplitude of each channel.

To reduce the antenna size, both antennas can be combined into a single aperture, as proposed in the literary works [6, 7]. An interleaved Rx/Tx combined aperture requires dual-band radiators, such as in the work of Jaschke *et al.* [8], and Tx-only radiators. The former need diplexers to separate Tx and Rx for full-duplex operation. One of the main issues with the Rx-/Tx-integrated array antennas is the Tx-leakage into the Rx-path. In other applications, such as wireless communications (e.g., 4 G or 5 G), Rx-signal degradation mainly results from intermodulation products [9, 10]. In Ka-band SatCom, this is of limited relevance due to the wide frequency spread. Here, the main degradation effect is the compression of the low-noise amplifier (LNA) by the Tx-signal. This results in an increased bit error rate, as shown in [11].

This contribution reports a frontend architecture for Rx-/Tx-integrated phased arrays at Ka-band. The available real-estate is dictated by antenna physics and, thus, imposes severe constraints on the design. Solutions have to be compact and simultaneously exhibit good electrical performance. A frontend circuit for an Rx/Tx dual-band element has been proposed in the work of Sieganschin *et al.* [12]. It relies on printed circuit board (PCB) technology and comprises an LNA, a compact diplexer, and a bandpass filter. The diplexer is electrically short to keep losses and, in turn, the noise figure low. The isolation is sufficiently high to prevent the LNA from being driven into compression. The remaining Tx-signal in the Rx-path is further suppressed by means of the filter. This architecture allows to maintain a low receiver noise figure in lossy substrates. The present work extends the results from the work of Sieganschin *et al.* [12] and explains the working principle and the performance of the passive components. Additionally, the frontend is extended to include the feed for the Tx-only antenna element. The proposed solution represents the unit cell of a full Rx-/Tx-integrated array with the interleaved grid from the work of Jaschke *et al.* [7]. The circuit is manufactured and then characterized by means of measurements.

The paper is organized as follows. “Frontend concept” section describes the concept. “LNA characterization” section briefly recalls the nonlinear effects of the LNA. “Passive components” section is devoted to the required passive components, i.e., diplexers, filters, and transitions, and reports their simulated and measured performances. “Low-noise frontend assembly” section discusses the whole frontend assembly for the dual-band and the Tx-only antenna

elements, summarizes the achieved measurement results, and compares the configuration to the state of the art. “Conclusion” section concludes the paper.

### Frontend concept

The interleaved Rx-/Tx-integrated antenna array is sketched in Fig. 1(a) [7]. It consists of Rx/Tx and Tx-only elements, which are placed  $\lambda_{30}/2 = 5$  mm apart on a rectangular grid,  $\lambda_{30}$  being the wavelength in vacuum at 30 GHz. This avoids grating lobes up to 30 GHz. The elements for Rx are thus separated by 7.1 mm on a rectangular grid rotated by  $45^\circ$ . This is less than half the vacuum wavelength up to 21.2 GHz. Figure 1(b) is a schematic representation of the whole arrangement. The array relies on a brick architecture and is realized in a modular way, each module consisting of a row of these antenna elements on a PCB with adequate feeds for Rx/Tx and Tx-only radiators. Figure 2 illustrates the simplified schematic representation of a module. The dual-band elements require a diplexer to separate the Rx and the Tx signals. The corresponding signal paths are connected to Rx- and Tx-BNs, which can be realized with commercially available integrated beamforming circuits, such as *AMWF-0109* and *AWS-0102* from *Anokiwave*. Figure 3(a) presents the frontend architecture of traditional Rx-/Tx-integrated antennas, such as reflector antennas. The required high isolation between Rx and Tx leads to an electrically large diplexer, in general, which is thus mostly realized in conventional waveguide technology to minimize losses.

In arrays realized in PCB technology, this approach is prohibitive due to the incurred increased losses. Indeed, the latter would degrade the noise figure, since the diplexer is at the LNA input. Figure 3(b) shows an alternative frontend architecture that allows to mitigate this problem in compact arrays. Instead of an electrically long diplexer with high isolation, a combination of a diplexer and a bandpass filter is used to achieve the total isolation. The diplexer is electrically short for low insertion loss. As this reduces the isolation, there is a significant Tx-leakage into the Rx-path, which possibly drives the LNA into compression. Thus, a compromise has to be found between the required isolation for low distortions and an acceptable noise figure, as was discussed in [11].

In addition, depending on its characteristics, the LNA could also amplify the Tx-signal in the Rx-path. Subsequent active components, such as amplitude tuners and phase shifters, could thus be driven into compression, as well. To prevent this, the spurious Tx-signal is attenuated by a bandpass filter. As this is connected to the LNA output, it has little impact on the receiver noise figure, even in case of a higher-order bandpass characteristic.

### LNA characterization

The frontend architecture is demonstrated with the amplifier QPA2626 from *Qorvo*, which features a very low-noise figure of 1.3 dB and a small signal gain of 25 dB at 20 GHz. The measured small-signal characteristics are plotted in Fig. 4(a). Here, port 1 is the input and port 2 the output of the amplifier. At 30 GHz, a gain of about 7 dB is observed. Two-tone measurement results are given in Fig. 4(b). Here, a small 20 GHz signal and a large 30 GHz signal are simultaneously applied to the LNA input. The power of the Tx-signal is varied and the phase distortion ( $\Delta\varphi_{Rx}$ ) and amplitude compression ( $\Delta A_{Rx}$ ) of the Rx-signal are measured. No significant phase distortion and amplitude compression are observed below  $-10$  dBm. Knowing the isolation

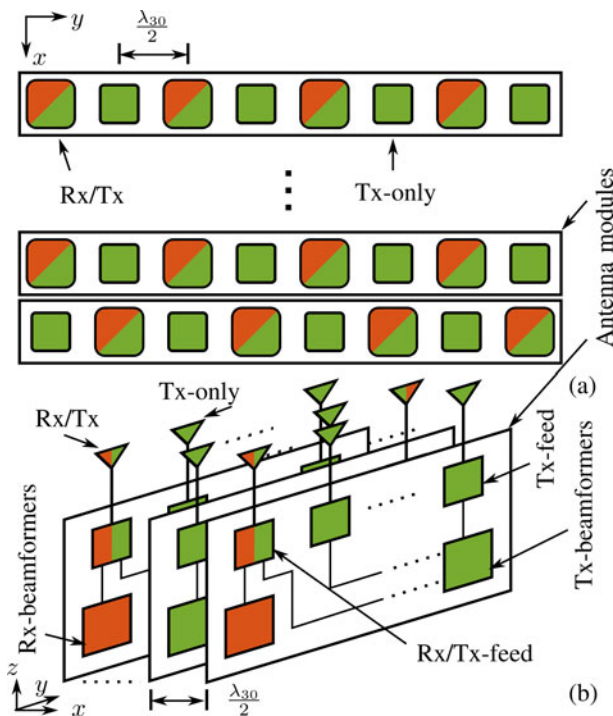


Fig. 1. Interleaved Rx/Tx phased array grid; (a) top view and (b) modular setup.

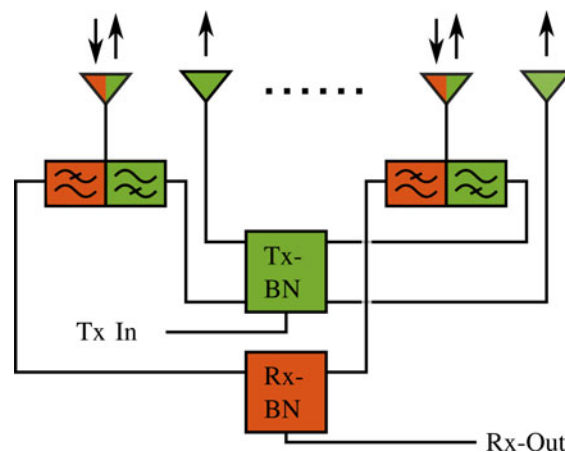


Fig. 2. Simplified frontend schematic representation of an antenna module.

of the diplexer, the maximum output power of the power amplifier (PA) can be determined.

### Passive components

This section discusses the diplexer and the bandpass filter. They are realized in substrate-integrated waveguide (SIW) technology and are compatible with dual-band radiators such as the one presented in [8]. The following also describes the transitions needed to connect these SIW-components.

### Diplexer

The diplexer is illustrated in Fig. 5. It is essentially the same as in [13], but with minor improvements to better cope with the

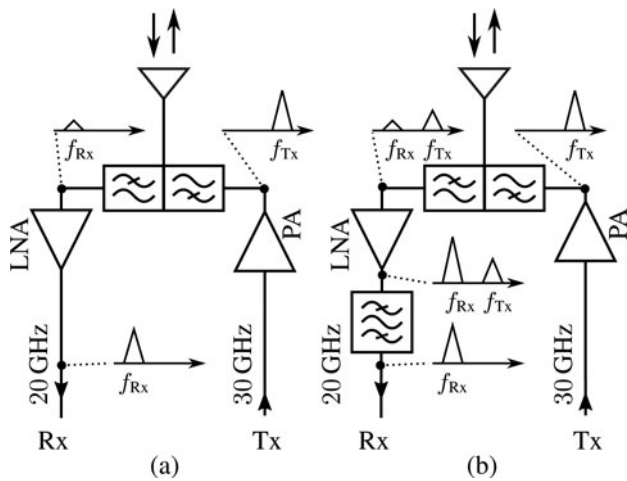


Fig. 3. (a) State of the art and (b) proposed frontend architecture for K-/Ka-band dual-band antenna element.

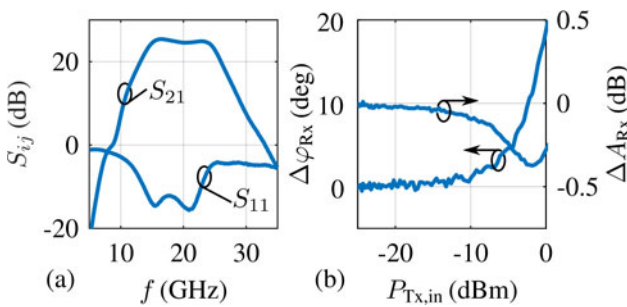


Fig. 4. (a) Small-signal characteristics and (b) two-tone measurement results of the LNA.

tolerance effects of the employed PCB technology. It is implemented with *Megtron 6* substrates from *Panasonic*. The permittivity  $\epsilon_r$  and the loss tangent  $\tan(\delta)$  at the considered frequencies are 3.62 and 0.005, respectively. **Figure 6** illustrates the concept of the proposed diplexer. It consists of two filters, one for Rx and one for Tx. The common antenna port is connected via a vertical SIW bifurcation, which is also a design element of both filters. An aperture inserted in the Rx-path couples two shorted SIW-stubs. These generate two transmission zeros at 30 GHz and block the Tx-signal in the Rx-path. The aperture is followed by a SIW-to-CPW transition similar to the one in [14] and which is also a design element of the Rx-filter. In the Tx-path, the bifurcation is connected to irises which serve matching purposes. The Tx-SIW is below the cutoff in the Rx-band, so that no further filtering is required here.

**Figure 5** depicts the model of the diplexer. The width  $w_{20}$  of the Rx-SIW and of the SIW of the common port is 5 mm. The width  $w_{30}$  of the Tx-SIW is chosen as 3.5 mm. The cutoff frequencies of the fundamental modes are 17 GHz and 25 GHz, respectively. Two cuts in the model revealed some details of the implementation.

The performance of the diplexer is presented in **Fig. 7**. The simulation of all passive components in this work is performed with the frequency domain solver of *CST Microwave Studio*. The measured isolation exceeds 40 dB in the Tx-band. The measured insertion loss is very low with 0.7 dB at the Rx-frequencies.

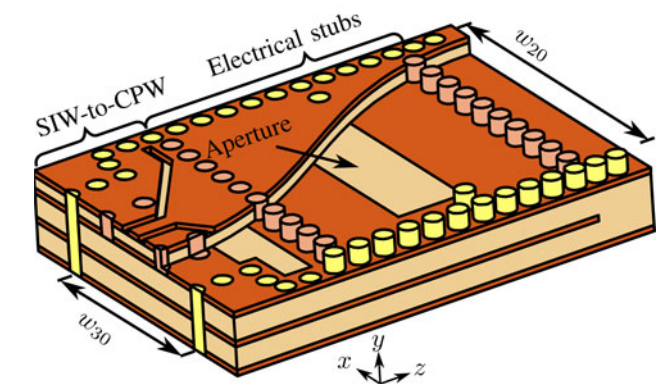
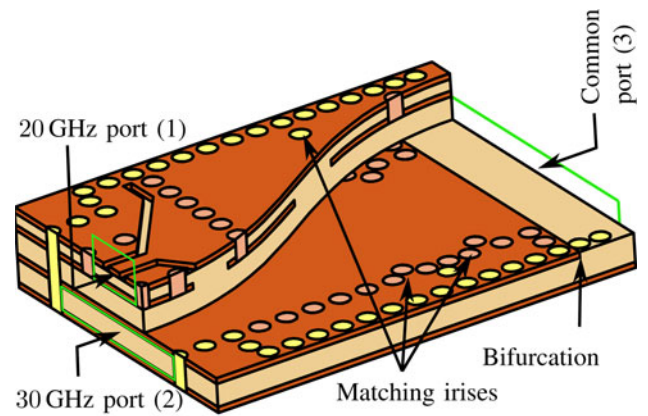


Fig. 5. Model of the diplexer with two different cutaway views.

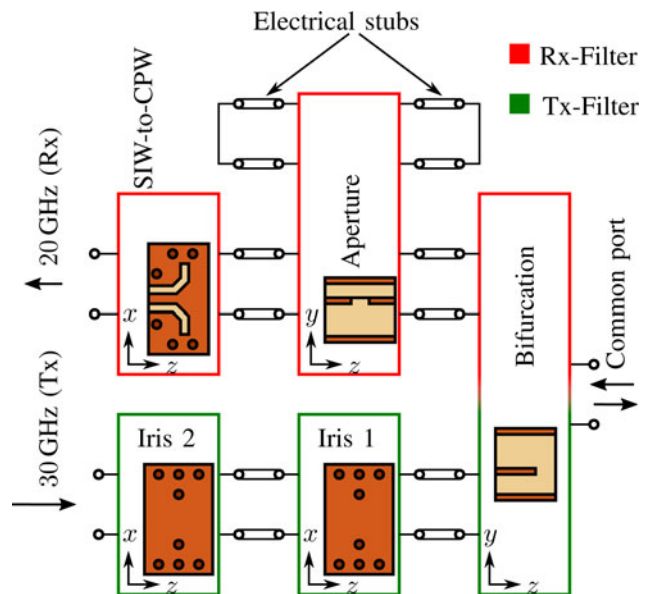
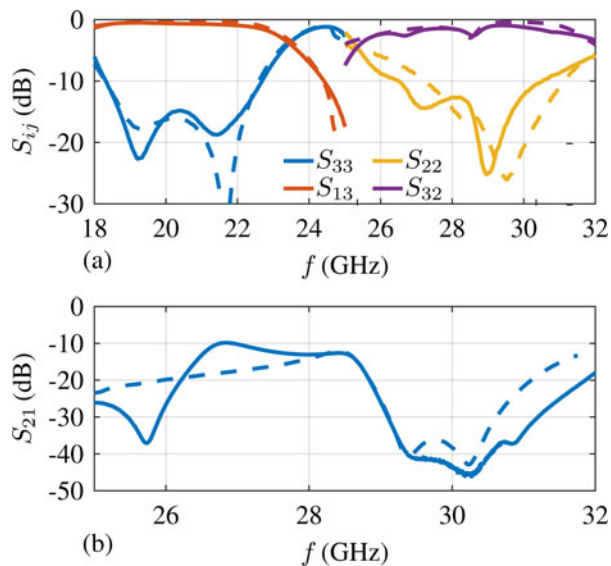


Fig. 6. Schematic representation of the diplexer.

**Bandpass filter**

The bandpass filter is realized as a fourth order SIW-filter with corner cavities as depicted in **Fig. 8(a)**. The lengths  $l_i$  and the widths  $w_i$  of the corresponding cavities adjust the resonant frequency. The total width  $w_1 + w_2$  has to be kept  $< 10$  mm to



**Fig. 7.** Simulated (dashed line) and measured (solid line) results of the diplexer. (a) Transmission and reflection coefficients  $S_{13}$ ,  $S_{32}$ ,  $S_{33}$ ,  $S_{22}$  and (b) transmission coefficient  $S_{21}$ .

comply with the array grid. With the iris displacements  $d_{ij}$  transmission zeros of the corner cavities can be placed in the Tx-band, as described in [15]. The parameters  $w_{ij}$  adjust the coupling of the source and of the load as well as between the resonators. A Chebyshev characteristic chosen for the filter response yields the symmetry plane shown in Fig. 8(a). The filter dimensions are determined by optimization. The simulated and measured results are plotted in Fig. 8(b). The measured insertion loss is 3.8 dB at 20 GHz and the isolation is about 60 dB at 30 GHz.

### CPW-to-SIW transition

The high integration density of the frontend requires different passive transitions. As the SIW components are quite large, it is preferable to place them in inner PCB layers and leave the top and bottom layers for the active components. This calls for adequate transitions between the layers. Figure 9 shows a model of a transition between a CPW and an SIW in inner layers. It is realized in two steps, i.e., with an intermediate stripline. This requires two blind vias and a taper, as shown in the figure. The taper parameters and the distance between the vias are adjusted in simulation. Due to technological constraints, a single blind via would possess a large diameter. This, in turn, would require more advanced matching techniques.

The design of the 20 GHz transition is validated with the back-to-back arrangement shown in Fig. 10. The simulated and measured results reported in Fig. 11 agree very well. The transition exhibits an input reflection of  $-10$  dB from 18 to 25.7 GHz and an insertion loss of  $2 \times 0.6$  dB at 20 GHz.

### SIW-to-SIW transition

A complex multilayer stack may require many different SIW-to-SIW transitions. Figure 12(a) shows the schematic representation of a transition between two SIWs with different height. It does not include any taper structures as in [16] or stepped impedances as in [17], and consists, instead, of an  $E$ -plane aperture, two stubs lines, and irises implemented with vias.

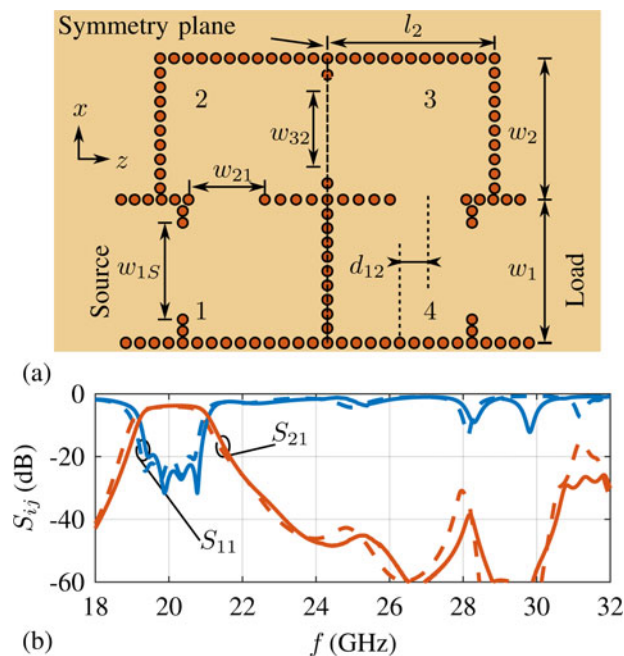


**Fig. 8.** (a) Layout of the corner cavity filter and (b) simulated (dashed line) and measured (solid line) results of the bandpass filter.

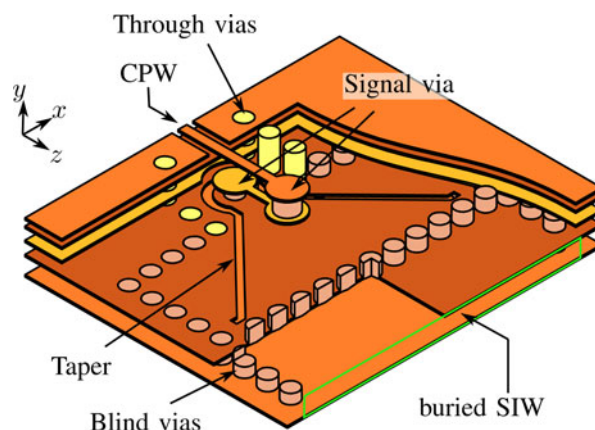


**Fig. 9.** Transition between CPW and buried SIW (two cut planes).

The change in height is achieved by connecting the SIWs through a bifurcation. The remaining ports are hereby terminated with short circuits implemented with a via fences. In general, the aperture coupling in conjunction with the different thicknesses leads to a field and impedance mismatch, which also affects the whole transition. The match is improved by adjusting the length of the stub lines and the width and position of the irises.

Figure 12(b) depicts the model of a transition from a thick SIW to a thin SIW for the Tx-signal. The measurements documented in Fig. 13 for a back-to-back arrangement demonstrate a 10 dB bandwidth reaching from 26.7 to 32 GHz and an insertion loss of  $2 \times 0.8$  dB at 30 GHz and thus agree very well with simulation.

### Low-noise frontend assembly

Figure 14 shows the PCB stack of the frontend. It is based on Megtron 6 laminates from Panasonic. This section discusses first

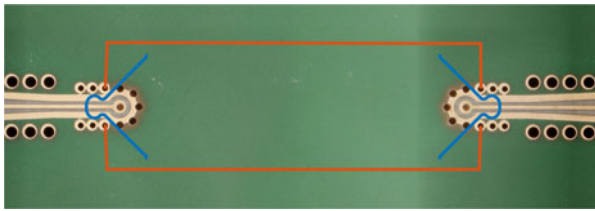


**Fig. 10.** Manufactured back-to-back transition from CPW to buried SIW. The positions of the SIW and of the taper are indicated by (red line) and (blue line), respectively.

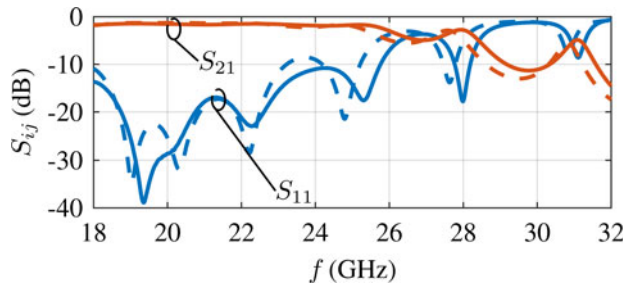


**Fig. 11.** Simulated (dashed line) and measured (solid line) results of the back-to-back CPW-to-SIW transition.

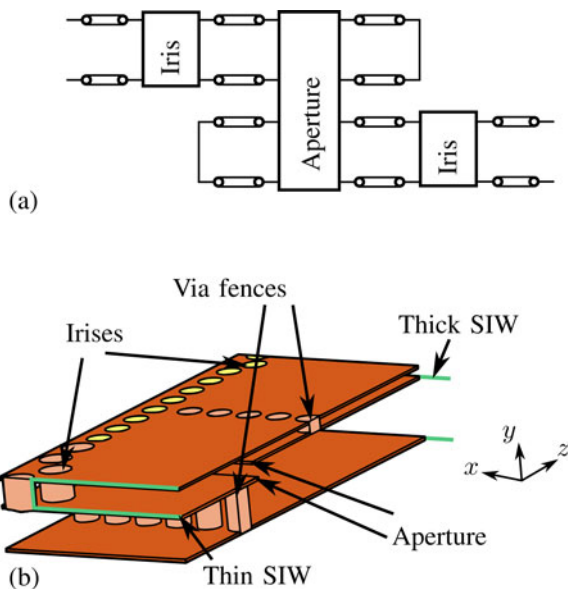


**Fig. 12.** (a) Schematic representation and (b) model of the SIW-to-SIW transition.

the frontend solution for the dual-band element and then that for the interleaved array grid.

**Subassembly for the dual-band elements**

Figure 15 shows the photograph of the frontend circuit for the dual-band element with the common port to feed the Rx/Tx element. The port numbering is the same as for the diplexer in Fig. 5. The red line represents buried via rows between the inner layers L4 and L5. They are accessed by the CPW-to-SIW transitions presented above.

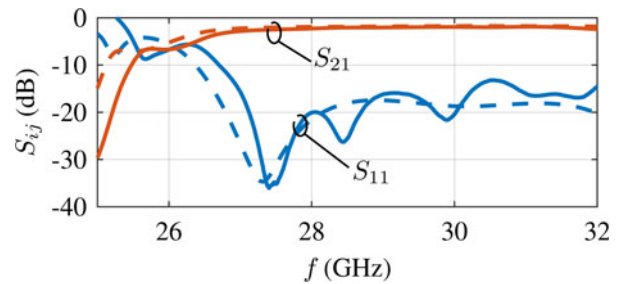


**Fig. 13.** Simulated (dashed line) and measured (solid line) results of the SIW-to-SIW transition in a back-to-back arrangement.



**Fig. 14.** Multilayer stack of the frontend assembly.

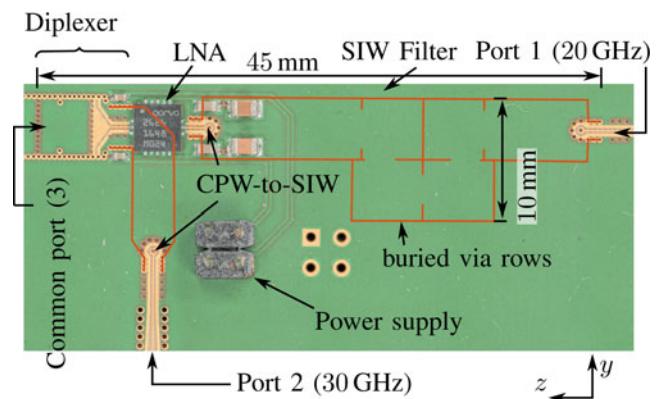


**Fig. 15.** Photograph of the manufactured dual-band element frontend.

The measured results are documented in Fig. 16. The small-signal gain between the diplexer input and the filter output is 20.5 dB at 20 GHz. The gain of the LNA is significantly offset by the filter losses. This agrees well with the measured characteristics of the individual components.

Nonetheless, with an LNA noise figure of 1.3 dB and the insertion loss of the diplexer, a noise figure as low as about 2 dB is achieved for the frontend in the 20 GHz passband (see Fig. 17). Additionally, the maximum PA output power for negligible Rx-signal compression is 30 dBm. The input reflection coefficient  $S_{33}$  of the cascaded circuit remains below about  $-10$  dB within the Rx-passband. The Tx transmission coefficient of the frontend corresponds to that of the diplexer. The isolation at 30 GHz is about 70 dB. It is lower than the summed isolations of all components. The reason is a finite parasitic coupling through fences between the buried Tx- and Rx-SIW. However, this can be easily remedied by adding more vias.

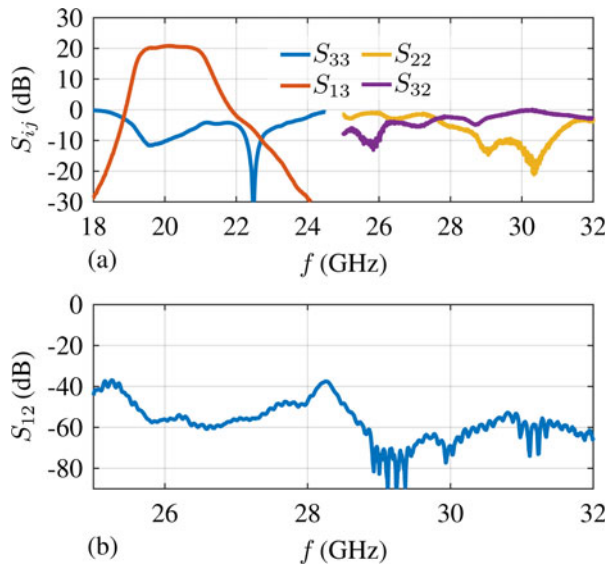


**Fig. 16.** Measured results of the frontend circuit. (a) Transmission and reflection coefficients  $S_{33}$ ,  $S_{22}$ ,  $S_{13}$ ,  $S_{32}$  and (b) transmission coefficient  $S_{12}$ .

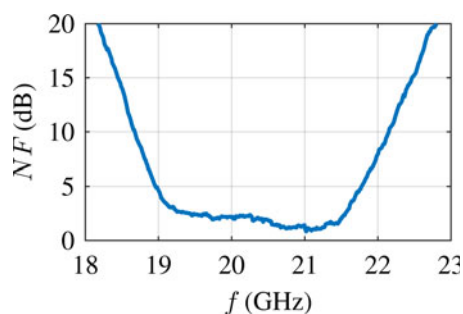


**Fig. 17.** Measured noise figure of the frontend circuit.

### Interleaved array frontend

Next, the presented Rx/Tx feed is extended to include the Tx-only element. The resulting circuit is presented in Fig. 18. The Tx-element is fed through the SIW-to-SIW transition from a thick SIW to a thin SIW. This creates space in the inner layer for the dual-band element Tx-path. The two Tx-paths in the stacked SIWs successively transition into CPWs on the PCB-surface, which will eventually connect the Tx-BN. The Rx-path remains the same as in Fig. 15.

The measured results of the two-port Tx-only feed and the Tx-path of the Rx/Tx feed are reported in Fig. 19. The port numbering refers to Fig. 18. The insertion loss for the Tx-only and for the combined Rx/Tx element is  $\sim 2$  and 2.9 dB, respectively. The increased losses in the Rx/Tx-channel result mainly from the longer path. The return loss is slightly decreased compared to Fig. 16(a) due to the cascaded passive components. The distance between the Rx/Tx and the Tx-only element is 5 mm and therefore complies with the array arrangement sketched in Fig. 1. Thus, the circuit is suitable as a unit cell of an antenna module, which will eventually contain significantly more elements.

Dual-polarization functionality is realized by stacking two such circuits with respect to layer L5. The resulting nine-layer PCB possesses active components on the top and on the bottom layers. It is suited to feed the two linearly polarized input ports of

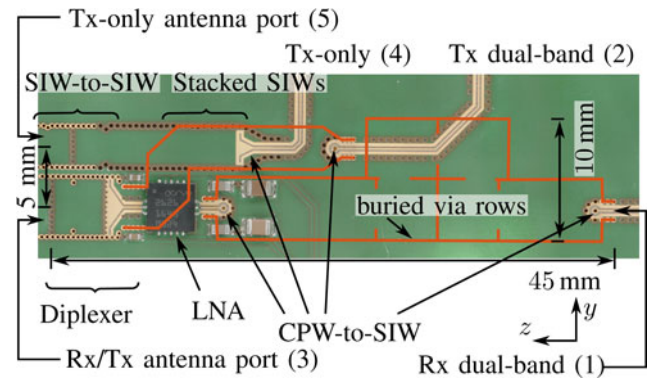


**Fig. 18.** Photograph of the frontend circuit for the interleaved array.

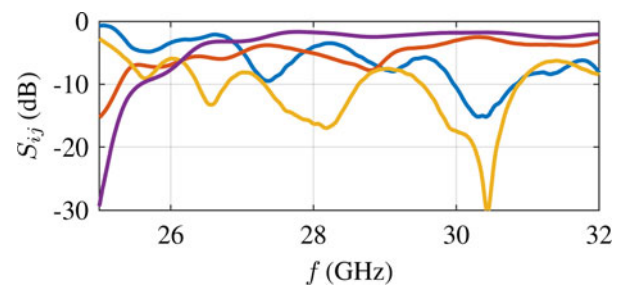


**Fig. 19.** Measured frontend performance.  $S_{22}$  (blue line) and  $S_{32}$  (red line) of the dual-band feed and  $S_{44}$  (yellow line) and  $S_{54}$  (purple line) of the Tx-only feed.

dual-polarized wide-band radiators such as in [8] which feature septum polarizers [18] to generate left- and right-handed circular polarization at the output.

The final array will be formed in accordance with link budget requirements by combining many such modules in a way similar to that in [19].

### Comparison with the state of the art

State-of-the-art phased arrays rely on two separate apertures with two orthogonal polarizations, as reported in the work of Weilow *et al.* [20] for Tx and in the work of Theunissen *et al.* [2] for Rx. A combined Rx/Tx aperture usually features switches for alternating Rx and Tx operation [4, 21, 22]. On the other hand, [23] presents a beamformer chip capable of full-duplex Rx/Tx with a noise figure of 3.2 dB. This, however, requires radiators with four inputs, two for Rx and two for Tx.

In contrast, together with commercially available BNs, the presented circuit enables full-duplex Rx/Tx operation of dual-polarized phased arrays.

### Conclusion

This work presents a low-noise frontend for interleaved Rx-/Tx-integrated SatCom phased arrays. The frontend feeds dual-band Rx/Tx elements and Tx-only elements. For the dual-band feed, the LNA is placed close to the antenna to reduce the insertion loss of the diplexer and, thus, the noise figure. LNA measurements are used to determine the maximum allowable PA output power. A bandpass filter follows the LNA to block the parasitic Tx-signal in the Rx-path. Measured and simulated results are

reported for the individual active and passive components. The assembled frontend exhibits a gain of 20.5 dB and an isolation of 70 dB. Although the circuit exhibits relatively high losses, the proposed system design allows to still maintain a noise figure of 2 dB only. For the Tx-path, an insertion loss of 2.9 dB is measured. The frontend thus complies with typical requirements of SatCom phased arrays in combination with BNs and represents a suitable unit cell for an active antenna module.

**Acknowledgement.** The authors wish to acknowledge for the funding and support of this work by the German Aerospace Center (DLR) on behalf of the German Federal Ministry of Economics and Technology (BMWi) under research contracts 50 YB 1707 and 50 RK 1926.

## References

1. Wei Low KK, Nafe A, Zihir S, Kanar T and Rebeiz GM (2019) A scalable circularly-polarized 256-Element Ka-Band phased-array SATCOM transmitter with  $\pm 60^\circ$  beam scanning and 34.5 dBW EIRP. *IEEE MTT-S International Microwave Symposium*, 1064–1067.
2. Theunissen W, Jain V and Menon G (2018) Development of a receive phased array antenna for high altitude platform stations using integrated beamformer modules. *IEEE MTT-S International Microwave Symposium*, 779–782.
3. Abdel-Wahab WM, Al-Saedi H, Mirza Alian EH, Raeis-Zadeh M, Ehsandar A, Palizban A, Ghafarian N, Chen G, Gharaee H, Nezhad-Ahmadi MR and Safavi Naeini S (2019) A modular architecture for wide scan angle phased array antenna for K/Ka mobile SATCOM. *IEEE MTT-S International Microwave Symposium*, 1076–1079.
4. Tabarani F, Boccia L, Purtova T, Shamsafar A, Schumacher H and Amendola G (2018) 0.25  $\mu\text{m}$  BiCMOS system-on-Chip for K-/Ka-Band satellite communication transmit-receive active phased arrays. *IEEE Transactions on Microwave Theory and Techniques* **66**, 2325–2339.
5. Min B-W and Rebeiz GM (2008) Single-ended and differential Ka-Band BiCMOS phased array front-ends. *IEEE Journal of Solid-State Circuits* **43**, 2239–2250.
6. Luo Q, Gao S, Chaloun T, Menzel W, Boccia L, Arneri E, Amendola G and Ziegler V (2013) Antenna array elements for Ka-band satellite communication on the move. *Proceeding Loughborough Antennas & Propagation Conference (LAPC)*, 135–139.
7. Jaschke T, Rohrdantz B, Mitto HK and Jacob AF (2016) Rx/Tx integration concepts for ground segment SatCom antenna arrays. *Proceedings German Microwave Conference (GeMIC)*, 27–30.
8. Jaschke T, Mitto HK and Jacob AF (2018) K/Ka-band dual-polarized SIW-Fed lens antennas for Rx/Tx integration. *International Journal of Microwave and Wireless Technologies* **10**, 627–634.
9. Kiayani A, Anttila L and Valkama M (2013) Modeling and dynamic cancellation of TX-RX leakage in FDD transceivers. *IEEE International Midwest Symposium on Circuits and Systems*, 1089–1094.
10. Gebhard A, Lang O, Lunglmayr M, Motz C, Kanumalli RS, Auer C, Paireder T, Wagner M, Pretl H and Huemer M (2019) A robust non-linear RLS type adaptive filter for second-order-intermodulation distortion cancellation in FDD LTE and 5 G direct conversion transceivers. *IEEE Transactions on Microwave Theory and Techniques* **67**, 1946–1961.
11. Sieganschin A, Jaschke T, Safi D and Jacob AF (2018) On the design of active Rx/Tx-diplexers with wide frequency spread. *Proceedings German Microwave Conference* 315–318.
12. Sieganschin A, Jaschke T and Jacob AF (2021) A compact low-noise frontend for Rx/Tx-integrated SatCom arrays. *Proceedings of the 2020 50th European Microwave Conference (EuMC)*, 820–823.
13. Sieganschin A, Jaschke T, Mitto HK, Lamann NJ, Waldhelm J and Jacob AF (2019) A compact low-loss multilayer SIW diplexer at K/Ka-band. *Proceedings German Microwave Conference (GeMIC)*, 51–54.
14. Chen X-P and Wu K (2009) Low-loss ultra-wideband transition between conductor-backed coplanar waveguide and substrate integrated waveguide. *IEEE MTT-S International Microwave Symposium*, 349–352.
15. Jaschke T, Rohrdantz B, Mohncke J-P and Jacob AF (2016) A Ka-band substrate-integrated waveguide diplexer with wide frequency spread. *IEEE MTT-S International Microwave Symposium*, 779–782.
16. Jaschke T and Jacob AF (2017) Novel multilayer SIW tapers synthesized using an extended transverse resonance method. *IEEE MTT-S International Microwave Symposium*, 715–718.
17. Jaschke T, Rohrdantz B and Jacob AF (2015) Dual-band stepped-impedance transformer to full-height substrate-integrated waveguide. *IEEE MTT-S International Microwave Symposium*, 367–370.
18. Chen M and Tsandoulas G (1973) A wide-band square-waveguide array polarizer. *IEEE Transactions on Antennas and Propagation* **21**, 389–391.
19. Kuhlmann K and Jacob AF (2010) Active 30 GHz antenna array for digital beamforming and polarization multiplexing. *IEEE MTT-S International Microwave Symposium*, 1276–1279.
20. Wei Low KK, Zihir S, Kanar T and Rebeiz GM (2020) A scalable switchable dual-polarized 256-Element Ka-Band SATCOM transmit phased-array with embedded RF driver and  $\pm 70^\circ$  beam scanning. *IEEE MTT-S International Microwave Symposium*, 821–824.
21. Chaloun T, Ziegler V and Menzel W (2016) Design of a dual-polarized stacked patch antenna for wide-angle scanning reflectarrays. *IEEE Transactions on Antennas and Propagation* **64**, 3380–3390.
22. Min B-W, Chang M and Rebeiz GM (2007) SiGe T/R modules for Ka-Band phased arrays. *IEEE Compound Semiconductor Integrated Circuit Symposium (CSIS)*, 1–4.
23. Tabarani F, Boccia L, Calzona D, Amendola G and Schumacher H (2020) Power-efficient full-duplex K/Ka-band phased array front-end. *IET Microwaves, Antennas & Propagation* **14**, 268–280.



**Anton Sieganschin** received the B.Sc. and M.Sc. degrees from the Hamburg University of Technology, Hamburg, Germany, in 2015 and 2017, respectively, where he is currently pursuing the Ph.D. degree at the Institute of High-Frequency Technology. His current research interest includes phased arrays, passive components, and component packaging.



**Thomas Jaschke** was born in Hamburg, Germany, in 1988. He received the B.Sc. and M.Sc. degrees from the Hamburg University of Technology, Hamburg, Germany, in 2010 and 2012, respectively. Until 2020, he was with the Institute of High-Frequency Technology, Hamburg University of Technology. He is currently pursuing his Ph.D. degree. Since 2020, he is a radar system engineer with Wärsilä

SAM Electronics. His current research interests include active radar systems, phased arrays, passive components, electromagnetic theory, and antenna measurements.



**Arne F. Jacob** received the Dr.-Ing. degree from the Technische Universität Braunschweig, Braunschweig, Germany, in 1986. From 1986 to 1988, he was a Fellow with CERN, the European Organization for Nuclear Research, Geneva, Switzerland. In 1988, he joined the Lawrence Berkeley Laboratory, University of California at Berkeley, Berkeley, CA, USA, for almost three years as a Staff Scientist with the Accelerator and Fusion Research Division. In 1990, he became a Professor at the Institut für Hochfrequenztechnik, Technische Universität Braunschweig. From 2004 until his retirement in April 2020, he was a Professor and Head of the Institut für Hochfrequenztechnik at the Technische Universität Hamburg, Hamburg, Germany. His current research interests include the design, packaging, and application of integrated (sub-)systems up to millimeter frequencies and the characterization of complex materials.